Hindawi
International Journal of Aerospace Engineering
Volume 2020, Article ID 8817902, 19 pages
https://doi.org/10.1155/2020/8817902

Research Article

Mathematical Model for Analyzing Heat Transfer Characteristics of Ablative Thermal Insulating Material

Junjie Gao,[1,2] Haitao Han,[1,2] Daiying Deng,[1,2] and Jijun Yu[1,2]

[1]*China Academy of Aerospace Aerodynamics, Beijing, China 100074*
[2]*Laboratory of Aerothermal Protection Technology for Aerospace Vehicles, Beijing, China 100074*

Correspondence should be addressed to Jijun Yu; jijuny@163.com

Received 14 March 2020; Revised 6 May 2020; Accepted 23 May 2020; Published 8 July 2020

Academic Editor: Desong Fan

A mathematical model based on minimal thermal resistance and equal law of specific equivalent thermal conductivity is developed to discuss the heat transfer characteristics of ablative thermal insulating material from the mesoscopic scale. Based on the statistical results of mesoscopic parameters, the microstructure unit cell model was established to analyze the influence rule of mesoscopic parameterization which includes the size, distribution, and positional relation of microsphere and fiber. The results show that the equivalent thermal conductivity decreases with the density, size, distribution area, and distance of microsphere and the space distance and volume fraction of fiber decreasing. Besides, the equivalent thermal conductivity will become larger when more quality of heat transfers along the fiber direction. Exploring the relationship between the macroscopic heat transfer process and the microstructure is meaningful for exploring the heat transfer behavior of thermal insulating material and improvement of the processing technology.

1. Introduction

With the acceleration of the flight speed of an aircraft, and the strong aerodynamic heating of a reentry aircraft, to ensure that the internal instruments are not burnt out, it is necessary to take effective measures of heat insulation. Ablative thermal protection is a widely used thermal protection method. The ablative thermal insulating material will change a lot with the processing of ablation; it includes the pyrolysis, carbonization, chemical reaction, surface ablation, and second reaction of pyrolysis gas. The process is very complicated, and the material property will change. The microstructure of the ablative thermal insulating material will also change in the process of ablation. For example, the porosity increases, matrix deposits, fiber orientation changes, and distribution of microsphere and fiber will also change. The heat transfer process is very complicated. Solid and gas conduction, gas convection, and radiation exist in the process of ablation. However, according to Skochdopole's research [1], when the diameter of a hole is less than four millimeters, the gas convection can be ignored. As the radiation is very complicated, here, we just consider the influence of microstructure on the solid and gas conduction mechanism at room temperature; this can help us better understand the influence of the microstructure parameter on the heat transfer mechanism. Combining with the microstructure changes during the process of ablation, we can better understand the relationship between the microstructure parameter and the heat transfer process, and it is very meaningful for the material process improvement.

Theoretical models of evaluating the thermal conductivity of composites mainly include effective medium approximation (EMA) and micromechanics method. The EMA method comes from the classical Maxwell model [2–4]; it is used in the electromagnetic field at the earliest. Then, several researches used it to get the thermal conductivity [5]. Fricke [6] extended the Maxwell model to ellipsoidal particles. Hasselman and Johnson [7] considered the effect of interface and particle size. Bruggeman [8–10] considered the thermal interaction to extend the Maxwell model to make it suitable for a variety of materials and high filler volume fractions. Every extended Bruggeman model considers the interfacial

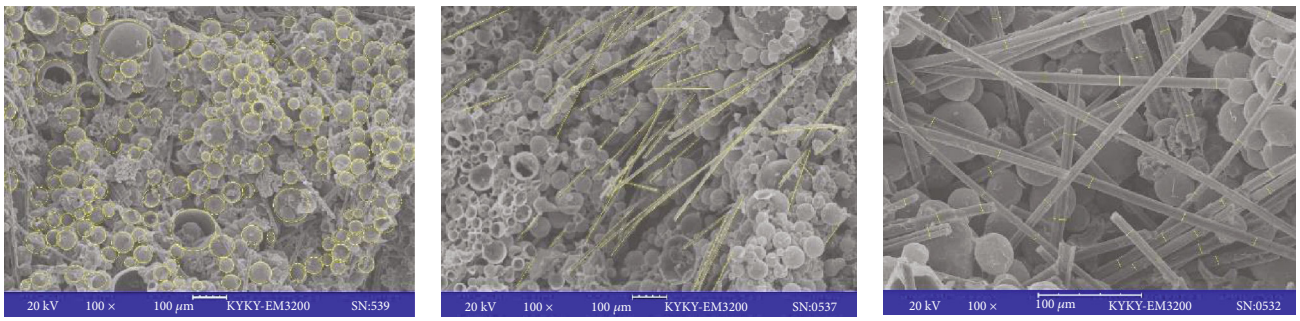

(a) (b) (c)

Figure 1: Microstructure image of thermal insulating material.

thermal resistance between particles and matrix [11, 12]. The micromechanics methods are based on the variational principle and the mean field approximation, for example, the Hashin-Shtrikman bounding model [13], Mori-Tanaka model [14], and Benveniste's model [15]. Besides, there are also some semiempirical models [16–18]. The Maxwell model and Fricke model can only be used in the lower volume fraction of particles which guarantees that the particles are apart from each other. The Hasselman-Johnson model, Bruggeman model, and every model considered the thermal resistance between fillers, but it is difficult to determine thermal resistance parameters, and sometimes, they should be dependent on experiment. The Hashin-Shtrikman bounding model is based on the variational principle; the Mori-Tanaka model and Benveniste's model are based on mean field approximation. They focus on one factor and are suitable for some specific material. Semiempirical models are dependent on experiment results, but they are often hard to realize.

The main theoretical models mostly focus on one factor about some kinds of material, and they have some limitation more or less. There is another theoretical model rooting from the electrical field. It is based on the law of minimal thermal resistance and the equal law of the specific equivalent thermal conductivity. Its main idea is to treat each section of microstructure as the thermal resistance. By analyzing the heat transfer mechanism, the series-parallel thermal resistance model is established; then, the equivalent thermal conductivity can be gotten. The challenge of this method is how to establish the unit cell model and the series-parallel thermal resistance model. But this method is convenient to consider the influence of microstructure on heat transfer characteristics. Literature reported so far gives some application of this model. For example, Zeng et al. [19], Cheng et al. [20], Li [21], Liang and Liu [22], Agrawal and Satapathy [23], and Devireddy and Biswas [24] used this model to predict the equivalent thermal conductivity.

The above theoretical models can all forecast the thermal conductivity of the composite and conform to the experiment values, but for the influence of mesoscopic parameters on the thermal conductivity of composites, there is less discussion. In the previous article of the authors [25], the mathematical and finite element models were used to analyze mesoscale heat transfer characteristics, and some of the mesoscopic parameterization was analyzed; however, it is not very detailed and full-scale. This paper discusses the heat transfer characteristics of thermal insulation materials with the establishment of a theoretical model, especially to explore the influence law of mesoscopic parameters from different scales. The purpose is to explore the relationship between material macroscopic heat transfer mechanism and material mesoscopic parameters and to provide reference for process design of ablative thermal insulating material.

2. Mesoscopic Observation and Statistical Analysis

Figure 1 shows the microstructure image of a kind of ablative thermal insulating material which is composed of hollow microspheres, resin matrix, fibers, and irregular pores. Statistics of the sizes of microspheres and fibers obtained through the Image-Pro Plus software are shown in Figure 2. Sizes of microspheres and fibers conform to the Gaussian distribution. The size range of microspheres and fibers can be obtained through the statistics results, and it is useful for the parameterization in the following passage that it determines the range of variables.

3. Mathematical Model

3.1. Mathematical Model of Microsphere Scale. The heat transfer model at the microsphere scale is established based on the law of minimal thermal resistance and the equal law of the specific equivalent thermal conductivity, as shown in Figure 3 [21]. In this article, this model is extended to be used for the heat transfer characteristics of thermal insulating material with complicated microstructure and the parameterization influence analysis.

Here, the unit cell model is the cube whose side length is a. The outer radius and inner radius of the microsphere are separately r_1 and r_2.

We consider the heat transfer of the unit cell in the z direction. There are three main ways of heat transfer: (1) heat conduction through solid and gas, (2) natural convection through the gas in the microsphere and the pores between the microspheres, and (3) thermal radiation passing through the inner and outer surfaces of the microsphere. Since the thermal conductivity of materials under normal temperature is researched, the amount of thermal radiation is very small,

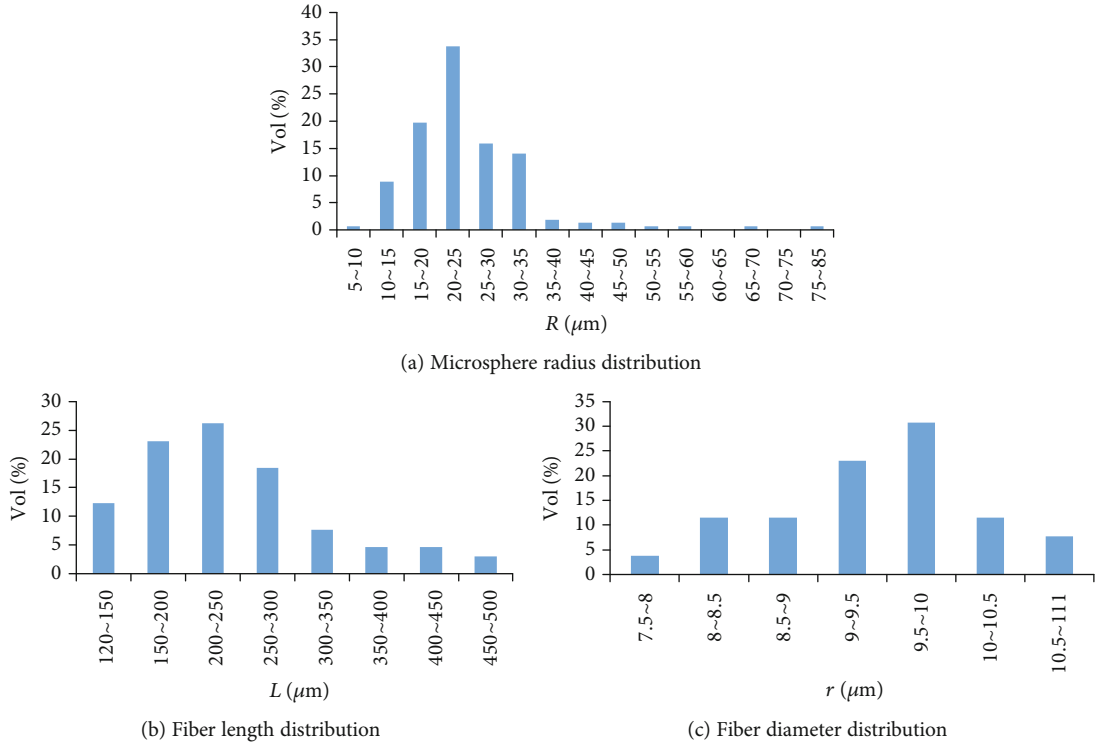

(a) Microsphere radius distribution

(b) Fiber length distribution

(c) Fiber diameter distribution

Figure 2: Statistical results of mesoscopic parameter.

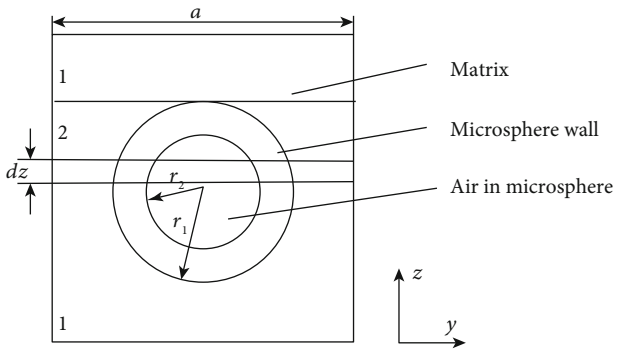

Figure 3: Microsphere unit cell model.

so it is ignored here. At the same time, the size of microspheres and the pores between microspheres is also small, so convection heat transfer is not considered in the modeling process. The following basic assumptions are established: (1) the microsphere and the matrix are in good contact; that is, the role of additional pores is not considered; (2) the microspheres are assumed to be periodically distributed; and (3) the microsphere scale is the micron scale, and the influence of the thin transition zone on the microsphere heat transfer is not considered. In this way, the equivalent thermal conductivity of the unit cell of a single microsphere can be predicted according to the statistical law [21].

The macroscopic equivalent thermal conductivity of materials is derived based on the heat resistance series and parallel law. As shown in Figure 3, the unit cell is divided into two parts. One part is the part without microspheres, and the height is $h_1 = a - 2r_1$; the other part is the part containing microspheres, and the height is $h_2 = 2r_1$.

Considering the integral along the z direction, the unit cell is divided into thin slices whose height is dz. For the first part,

$$k_1 = k_m. \tag{1}$$

For the second part, it is obtained by the Fourier law:

$$k_2 = \frac{Q_m + Q_g + Q_b}{(dT/dz) \cdot S}, \tag{2}$$

where S is the area of the cross-section perpendicular to the heat transfer direction, Q_m is the quantity of conduction heat of the matrix in the second part, Q_g is the quantity of conduction heat of the air inside the microsphere, and Q_b is the quantity of conduction heat of the microsphere wall. The expressions of each quantity of conduction heat are as follows:

$$\begin{cases} Q_m = k_m \dfrac{dT}{dz} S_m, \\ Q_g = k_g \dfrac{dT}{dz} S_g, \\ Q_b = k_b \dfrac{dT}{dz} S_b. \end{cases} \tag{3}$$

Then,

$$k_2 = k_m \frac{S_m}{S} + k_g \frac{S_g}{S} + k_b \frac{S_b}{S}. \tag{4}$$

The average thermal conductivity of each part is as follows:

$$\begin{aligned} \bar{k}_1 &= \frac{1}{h_1}\int_0^{h_1} k_1 dz = k_m, \\ \bar{k}_2 &= \frac{1}{h_2}\int_0^{h_2} k_2 dz = \frac{1}{h_2}\int_0^{h_2}\left(k_m \frac{S_m}{S} + k_g \frac{S_g}{S} + k_b \frac{S_b}{S}\right) dz \\ &= \frac{\left(k_m V_m + k_g V_g + k_b V_b\right)}{h_2 S}. \end{aligned} \tag{5}$$

The thermal resistance of the two parts are

$$\begin{aligned} R_1 &= \frac{h_1}{\bar{k}_1 S}, \\ R_2 &= \frac{h_2}{\bar{k}_2 S}. \end{aligned} \tag{6}$$

Since the heat is transferred along the z direction and it is in a series structure, the total thermal resistance and the equivalent thermal conductivity of the composite are separately

$$\begin{aligned} R_{\text{total}} &= R_1 + R_2, \\ k_z &= \frac{a}{R_{\text{total}} S} = \frac{a}{(R_1 + R_2) S}. \end{aligned} \tag{7}$$

Then,

$$\begin{aligned} k_z &= \frac{a}{S}\left(\frac{h_1}{k_m S} + \frac{h_2^2}{k_m V_m + k_g V_g + k_b V_b}\right)^{-1}, \\ V_m &= h_2 a^2 - \frac{4}{3}\pi r_1^3, \\ V_g &= \frac{4}{3}\pi r_2^3, \\ V_b &= \frac{4}{3}\pi\left(r_1^3 - r_2^3\right). \end{aligned} \tag{8}$$

The volume fraction of microsphere is

$$\varphi_s = \frac{(4/3)\pi r_1^3}{a^3} = \frac{4\pi}{3}\cdot\left(\frac{r_1}{a}\right)^3. \tag{9}$$

The relationship between the radius inside and outside of microspheres is

$$V_g \rho_g + V_b \rho_b = V_s \rho_s. \tag{10}$$

Besides,

$$\begin{aligned} V_b &= V_s - V_g, \\ r_2 &= r_1 \cdot \left(\frac{\rho_b - \rho_s}{\rho_b - \rho_g}\right)^{1/3}. \end{aligned} \tag{11}$$

Then,

$$\begin{aligned} k_z = \Bigg\{ &\frac{1 - (6\varphi_s/\pi)^{1/3}}{k_m} + \left[\frac{k_m}{2}\left(\frac{4\pi}{3\varphi_s}\right)^{1/3} + \frac{\pi}{3}\left(\frac{3\varphi_s}{4\pi}\right)^{1/3}\right. \\ &\cdot \left.\left(\frac{k_g(\rho_b - \rho_s)}{\rho_b - \rho_g} + \frac{k_b\left(\rho_s - \rho_g\right)}{\rho_b - \rho_g} - k_m\right)\right]^{-1}\Bigg\}^{-1}. \end{aligned} \tag{12}$$

The density of air is relatively small compared with the other components, so it can be ignored. Therefore, equation (12) can be simplified as

$$\begin{aligned} k_z = \Bigg\{ &\frac{1 - (6\varphi_s/\pi)^{1/3}}{k_m} + \left[\frac{k_m}{2}\left(\frac{4\pi}{3\varphi_s}\right)^{1/3} + \frac{\pi}{3}\left(\frac{3\varphi_s}{4\pi}\right)^{1/3}\right. \\ &\cdot \left.\left(\frac{\left(k_b - k_g\right)\rho_s}{\rho_b} + k_g - k_m\right)\right]^{-1}\Bigg\}^{-1}. \end{aligned} \tag{13}$$

The above is the process deriving the equivalent thermal coefficient of thermal conductivity of the microsphere scale based on the law of minimal thermal resistance and the equal law of the specific equivalent thermal conductivity. At the fiber scale, we use the same method to get the macroscale thermal coefficient of thermal conductivity. The results of this theoretical method are verified by experimental results in literature [25]; thus, the correctness of this theory is certified. So, the method is used for the following discussion.

3.2. Heat Transfer Model of Matrix and Porosity. It can be seen from Figure 1 that there are four mesoscopic structures, namely, microspheres, matrix, fibers, and pores. At the microsphere scale, the heat transfer between matrix and pores is rather complicated. Based on the observation results of mesoscopic structure images and the actual possible heat transfer situation, several heat transfer models of matrix and pores are established.

3.2.1. Parallel Model of Microsphere and Matrix. It can be seen from Figure 4 that in the process of heat transfer, most of the quantity of heat is transferred along the microsphere wall and the matrix outside the microsphere, so it is approximate to a parallel heat transfer structure. Here, a parallel heat transfer model between the matrix and the pores can be adopted [26], and the expression is

$$k_m = k_{m0}\frac{\varphi_{m0}}{\varphi_{m0} + \varphi_g} + k_g \frac{\varphi_g}{\varphi_{m0} + \varphi_g}. \tag{14}$$

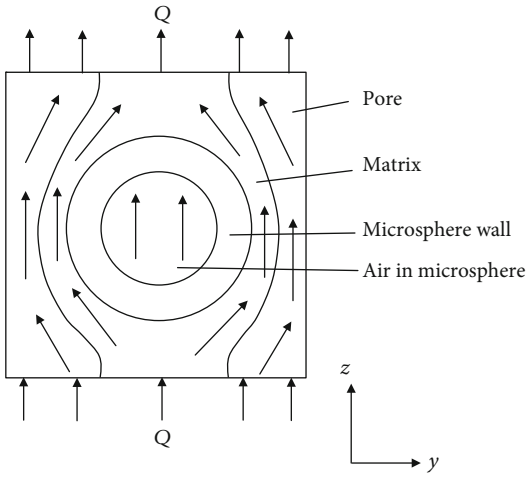

Figure 4: Heat transfer diagram of pores and matrix.

In equation (14), k_m is the thermal conductivity of the new equivalent matrix obtained in the parallel model between the pores and the matrix, k_{m0} is thermal conductivity of the resin matrix, k_g is the thermal conductivity of air, φ_g is the value of porosity, and φ_{m0} is the volume fraction of the resin matrix.

3.2.2. Spherical Pore Inclusion. The actual pores mostly exist among the microspheres, and they are irregular-shaped; here, they are assumed to be spherical pore inclusions. The established unit cell model is shown in Figure 5. The side length of the unit cell is a, and the radius of the spherical pore is r; the equivalent thermal conductivity is derived by the series-parallel method.

The equivalent thermal conductivity of spherical pore inclusion is

$$k_z = \frac{a}{S}\left(\frac{h_1}{k_m S} + \frac{h_2^2}{k_m V_m + k_g V_g}\right)^{-1}, \tag{15}$$

$$h_2 = 2r, \tag{16}$$

$$h_1 = a - 2r, \tag{17}$$

$$V_m = a^2 h_2 - \varphi_g a^3, \tag{18}$$

$$V_g = \varphi_g a^3, \tag{19}$$

$$S = a^2, \tag{20}$$

$$\varphi_g = \frac{4\pi r^3}{3a^3}. \tag{21}$$

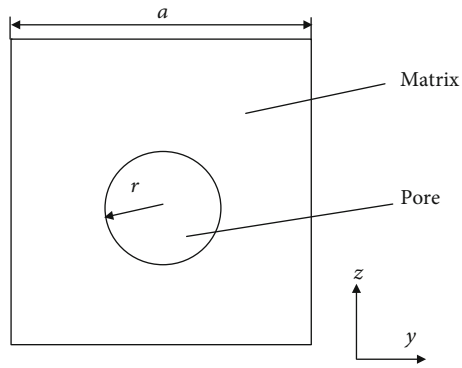

Figure 5: Spherical pore model.

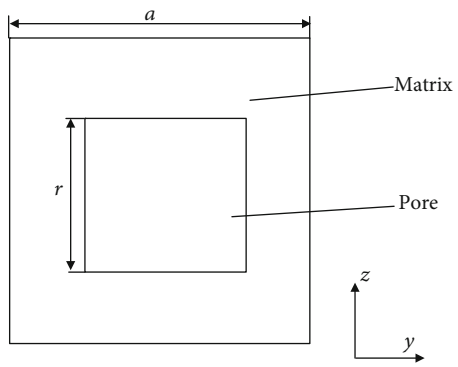

Figure 6: Cubic pore model.

Then,

$$k_z = \left\{\frac{1 - \left(6\varphi_g/\pi\right)^{1/3}}{k_m} + \frac{1}{k_m\left(\pi/6\varphi_g\right)^{1/3} + (\pi/3)\left(3\varphi_g/4\pi\right)^{1/3}\left(k_g - k_m\right)}\right\}^{-1}. \tag{22}$$

3.2.3. Cubic Pore Inclusion. It is assumed that the pores are cubes, as shown in Figure 6. The side length of the unit cell is a, and the side length of the cubic pore is r.

The expression of thermal conductivity is the same as formula (15), where

$$\begin{aligned} h_2 &= r, \\ h_1 &= a - r, \\ V_g &= r^3, \\ V_m &= a^2 r - r^3, \\ \varphi_g &= \frac{r^3}{a^3}. \end{aligned} \tag{23}$$

Table 1: Result comparison of different heat transfer models of matrix and porosity.

Heat transfer model of matrix and porosity	Thermal conductivity (W/(m·K))		
	A	B	C
Parallel model	0.1084	0.2065	0.1362
Spherical pore inclusion model	0.1168	0.2019	0.1382
Cubic pore inclusion model	0.1280	0.2181	0.1515

Substituting into formula (15), we can get

$$k_z = \left\{ \frac{1-\varphi_g^{1/3}}{k_m} + \frac{1}{k_m\left(1/\varphi_g\right)^{1/3} + \left(k_g - k_m\right)\varphi_g^{1/3}} \right\}^{-1}. \quad (24)$$

The results of the above three models are listed in Table 1. A, B, and C are three kinds of ablative thermal insulating material.

It can be seen from Table 1 that the results of the parallel model and the spherical pore inclusion model are relatively close, while the results of the cubic pore inclusion model are somewhat different from the former two models. It is because the actual pore structure is irregular, and the angular shape of the cubic pore is relatively clear, so it is not quite consistent with the actual situation. Among the three models, the parallel model is relatively simple and more consistent with the real heat transfer mechanism. Therefore, the parallel model is used to represent the heat transfer mechanism between the pores and the matrix.

4. Parametric Analysis

It can be seen from the microstructure images of ablative thermal insulating materials in Figure 1 and the statistical results in Figure 2 that the length scale of fibers is much larger than that of microspheres and pores, so the analysis method of two scales can be adopted here. From the microsphere scale, the size and distribution of microspheres are random, but from the fiber scale, the influence of microsphere randomness is weak as the fiber size is much larger compared with the microsphere size. Besides, investigating the influence of microspheres and fiber parameters separately can analyze the influence of different parameters more accurately.

4.1. Parameterization Influence Rule of Microsphere Scale. Due to the different position relationships between microspheres, the size of microspheres, and the changes in distribution, the transfer of heat flow will be affected, which will affect the transfer process of heat. In this way, the equivalent thermal conductivity of the calculated unit cell will be different.

4.1.1. The Density of Microspheres. In the actual material production process, the density of microspheres cannot be obtained accurately, and due to the influence of material technology, the wall thickness of each microsphere will change, so its density is a variable quantity, generally ranging from 200 to 400 kg/m^3. The following discussion is about the change of the equivalent thermal conductivity when the density of microsphere changes. When the density of microspheres changes, the volume content of each component also changes, but the mass content of each component and the density of other components remain unchanged. Taking these factors into consideration, the curve of the change of equivalent thermal conductivity with the density of microspheres is shown in Figure 7.

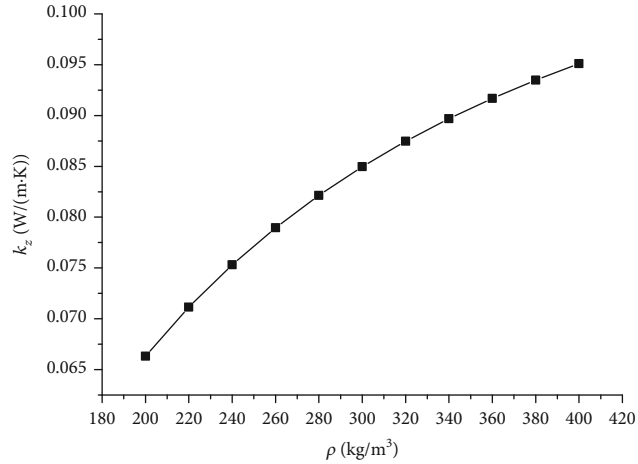

Figure 7: Variation of equivalent thermal conductivity with microsphere density.

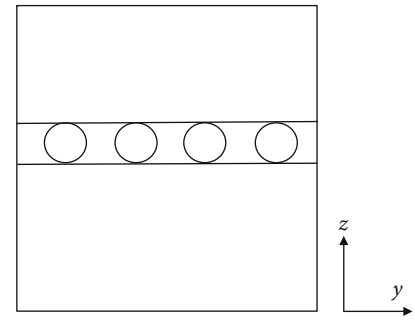

Figure 8: Multiple microsphere distribution.

It can be seen from Figure 7 that the equivalent coefficient of thermal conductivity increases with the increasing density of microsphere. It is because the microsphere is a hollow structure; larger density means larger volume of the microsphere wall and less gas inside the microspheres. So, the quantity of heat can be transferred more through the microsphere wall, and then, it can get larger equivalent thermal conductivity. So, in order to increase heat insulating performance, the density of microspheres should be smaller. However, when the density of microspheres is smaller, the microsphere wall is thinner and the mechanical strength is lower. So, the thermal insulating performance should be improved under the condition of ensuring the mechanical strength.

4.1.2. Microsphere Size. The influence of microsphere size on its heat transfer performance is worth studying. Here we assume that the size of microspheres is the same in the same model. As shown in Figure 8, microspheres are distributed on the plane whose coordinate z is zero. The change of the equivalent thermal conductivity along the z direction is discussed. The equivalent thermal conductivity is derived below. And n is the number of microspheres of each model and the total volume fraction of microspheres remains the same.

The equivalent thermal conductivity of z direction is as follows:

$$k_z = \left\{ \frac{1-(6\varphi_s/(n\pi))^{1/3}}{k_m} + \left[\frac{k_m}{2}\left(\frac{4\pi n}{3\varphi_s}\right)^{1/3} + \frac{n\pi}{3}\left(\frac{3\varphi_s}{4\pi n}\right)^{1/3} \cdot \left(k_g \cdot \frac{\rho_b-\rho_s}{\rho_b-\rho_g} + k_b \cdot \frac{\rho_s-\rho_g}{\rho_b-\rho_g} - k_m \right) \right]^{-1} \right\}^{-1}. \tag{25}$$

The value of n changes from 1 to 10, that is, under the condition that the volume fraction of the microspheres remains unchanged, the number of microspheres increases, and the volume of each microsphere decreases. The equivalent thermal conductivity of the unit cell varies with the number of microspheres, as shown in Figure 9.

It can be seen in Figure 9 that the microspheres distribute on the same plane, when the number of microspheres increases on the condition that the total volume of microspheres remains unchanged and the equivalent thermal conductivity of z direction decreases. The reason is that when the number of microspheres increased, the size of microsphere diminished. The matrix between microspheres decreases, the hollow microspheres will obstruct heat transfer path,

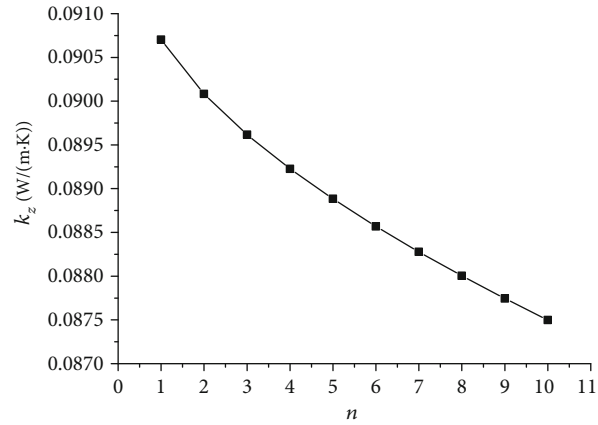

Figure 9: Variation of equivalent thermal conductivity with the number of microspheres.

and the thermal conductivity of microspheres is very low, so the thermal conductivity of z direction decreases when the size of microspheres decreases.

4.1.3. Microsphere Distribution Range. It can be seen from Figure 8 that the center of the microspheres is randomly distributed in a plane. The equivalent thermal conductivity which is perpendicular to the plane will decrease when the size of the microsphere decreases. If the size and number of the microspheres remain unchanged, the distribution area keeps expanding. In other words, when the distribution range of the microspheres increases from a certain height value (greater than the diameter of the spheres) to the whole height of the unit cell model which is shown in Figure 8, the change of the equivalent thermal conductivity of the unit cell is

$$k_z = \left\{ \frac{1-z}{k_m} + \frac{z^2}{zk_m + v_f\left(k_g\left((\rho_b-\rho_s)/\left(\rho_b-\rho_g\right)\right) + k_b\left(\left(\rho_s-\rho_g\right)/\left(\rho_b-\rho_g\right)\right) - k_m\right)} \right\}^{-1}, \tag{26}$$

where z is the proportion of the distribution area; z equals to 1 means the microspheres distribute in all of the unit cell. The variation curve of the equivalent thermal conductivity of the unit cell model changing with z is shown in Figure 10.

It can be seen in Figure 10 that when the number and the size of microspheres remain unchanged, the thermal conductivity along the z direction increases with the distribution area increase of microspheres. This is because when the microsphere distribution area is small, its configuration will be relatively dense which blocks the transfer of heat. When the distribution area of microsphere increases, the distribution of the microspheres is relatively dispersed and the heat can be transferred through the matrix between the microspheres, so the equivalent thermal conductivity of the unit cell is relatively large. This effect is particularly pronounced when the distribution increase is fast at first and then increases slowly.

4.1.4. The Distance between Microspheres. The microstructure of ablative thermal insulating material is that the microspheres distribute in the matrix, so the distance between the microspheres varies greatly. The influence of the distance between the microspheres on the thermal conductivity is discussed below. The established model is shown in Figure 11. The influence of the distance in z direction on the thermal conductivity is considered. It is assumed that the distance between the outer wall of microspheres along the z direction is z. Obviously, from the derivation process of thermal

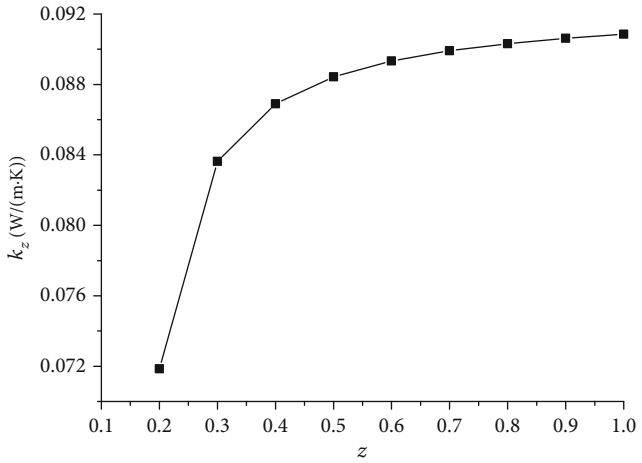

Figure 10: Variation of equivalent thermal conductivity with microsphere range.

conductivity, it can be seen that when the distance of z direction changes, the thermal conductivity along the x and y directions remains unchanged. The thermal conductivity

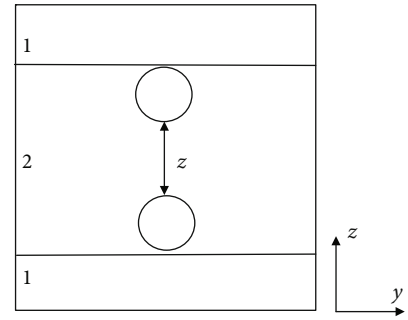

Figure 11: Distribution model of two microspheres.

only depends on the total volume fraction of the two microspheres. The influence of microsphere distance on thermal conductivity is discussed below.

It is supposed that the outer radius of the microsphere is r_1, the inner radius of the microsphere is r_2, the volume fraction of the microsphere is φ_s, the unit cell is the cube whose side length is a, and the equivalent thermal conductivity along the z direction is

$$k_z = \left\{ \frac{a - z - 4r_1}{k_m a} + \frac{(z + 4r_1)^2}{k_m a(z + 4r_1 - \varphi_s a) + \varphi_s a^2 \left(\left(\left(k_g(\rho_b - \rho_s) \right) / \left(\rho_b - \rho_g \right) \right) + \left(\left(k_b \left(\rho_s - \rho_g \right) \right) / \left(\rho_b - \rho_g \right) \right) \right)} \right\}^{-1}. \quad (27)$$

The distance value range of two microspheres is $z \in [0, a - 4r_1]$, and the length value of the unit cell is $a = 500\,\mu$m. When the microsphere is large enough, the two microspheres could not appear as shown in Figure 12, so the microsphere volume fraction is taken as 5% here. So, the value range of z is $z \in [0, 137]$, and thermal conductivity of z direction with respect to the distance between microspheres is shown in Figure 12.

It can be seen from Figure 12 that when the distance between two microspheres along z direction increases, the equivalent thermal conductivity of the unit cell along z direction increases. This result is in accord with what is shown in Figure 10. Here, we take the distance of two microspheres as variables, so we can study the influence between microspheres on the equivalent thermal conductivity more targeted.

4.2. Analysis of Heat Transfer Characteristics at Fiber Scale. The heat transfer characteristics at the microsphere scale have been discussed above. When the unit cell model is established at the fiber scale, the problem is equivalent to the case of fiber inclusion in a kind of homogeneous matrix.

From Figure 1, we can see that most of the fibers are straight and only a few of the fibers are bent regarding this kind of ablative thermal insulating material. This research is based on the microstructure of this kind of ablative thermal insulating material. So, we take the fibers as cylinder, and it is reasonable. For other materials, if most of fibers are bent, the model should be improved.

4.2.1. The Influence of Fiber Size. The shape of the fiber is generally cylindrical, but the fiber with the same volume content can be made into thin and long type or short and thick type.

The influence of the crudeness or fineness of the fiber on its thermal conductivity is discussed through the inclusion of a single fiber; the unit cell model considering the fiber size is shown in Figure 13.

(1) When the heat transfer direction is along the direction of the fiber, its thermal conductivity is expressed as

$$k_f = \left(\frac{a - l}{k_m a} + \frac{a l^2}{k_m (a^2 l - \pi r^2 l) + k_f \pi r^2 l} \right)^{-1} \quad (28)$$

(2) When the heat transfer direction is perpendicular to the direction of fiber, its thermal conductivity is expressed as

$$k_t = \left(\frac{a - 2r}{k_m a} + \frac{4 a r^2}{k_m (a^2 2r - \pi r^2 l) + k_f \pi r^2 l} \right)^{-1} \quad (29)$$

In the process that the fiber changes from slender to short and thick, the bottom radius r changes from small to large,

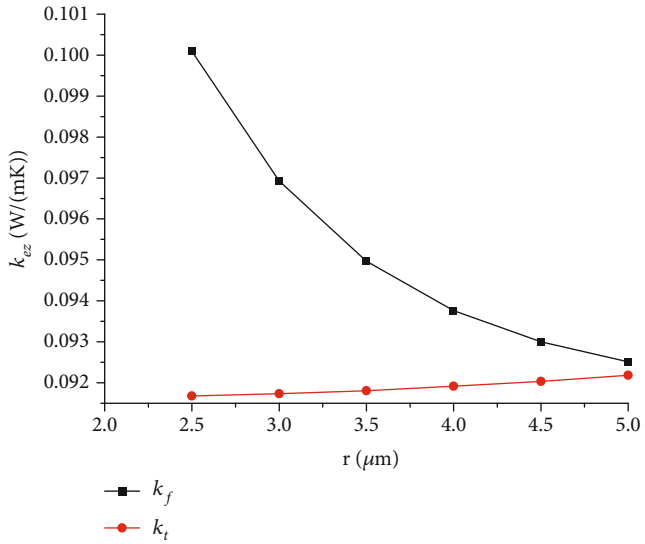

Figure 12: Variation of equivalent thermal conductivity with fiber size.

the length of the fiber can be determined based on the fiber volume invariability, and its variation law is shown in Figure 14. The longer the heat transfer path along the direction of the fiber, the greater the thermal conductivity.

4.2.2. Discussion of the Position Relationship between Fibers

(1) Several Cases of Positional Relationships between Fibers. The orientation, distribution, and position relationship of the fibers have great influence on the heat transfer characteristics. The influence of the relationship between two fibers on heat transfer characteristics is discussed below. Figure 15 is the unit cell model of the relationship between two fibers.

The position relationship between two fibers is represented by the distance between the fiber centers in three directions and the angle, that is, (x, y, z, θ). The average distance between two fibers is $\bar{s} = (a - 2d)/3$; the angle range between two fibers is $[0, \pi]$. The number of the two fibers is 1 and 2. The middle point of fiber 1 is $A(x_A, y_A, z_A)$, the middle point of fiber 2 is $B(x_B, y_B, z_B)$, and the angle of the two fibers is denoted as θ.

The distance between the two fibers is expressed as the distance between the midpoints:

$$s = \sqrt{(x_A - x_B)^2 + (y_A - y_B)^2 + (z_A - z_B)^2}. \quad (30)$$

The projection of fiber distance on three coordinate axes, that is, the distances in three directions, is, respectively,

$$\begin{cases} x = |x_A - x_B|, \\ y = |y_A - y_B|, \\ z = |z_A - z_B|. \end{cases} \quad (31)$$

The angle between the two fibers is complicated. As shown in Figure 16, the orientation of the two fibers is variable. When the midpoint of the two fibers is determined and the fiber rotates at any angle around the midpoint, the trajectories of the two endpoints of the fibers are spherical, denoted as spherical surface 1 and spherical surface 2.

When the distance between the two midpoints of the two fibers is greater than the length of the fiber, the sphere formed by the two ends of the fibers does not intersect, no matter what the angle is between the two fibers.

But in fact, the unit cell model is small and the fibers are always long enough which can intersect with each other. When the two spherical surfaces locate at the two corner points of the unit cell, the distance between the midpoints of the two fibers reaches the maximum.

Then,

$$A\left(\frac{l}{2}, \frac{l}{2}, \frac{l}{2}\right), \quad B\left(\frac{a-l}{2}, \frac{a-l}{2}, \frac{a-l}{2}\right). \quad (32)$$

When two fibers have one end in the volume formed by the intersection of two spheres, the two fibers can intersect; otherwise, the two fibers cannot intersect.

As shown in Figure 16(b), two fibers meet at the endpoints. And as shown in Figure 16(c), two fibers intersect with each other. The expression of the space angle between the two fibers is derived as follows.

It is assumed that the coordinate of any point on spherical surface 1 is $A_1(x_1, y_1, z_1)$; the coordinate of any point on spherical surface 2 is $B_2(x_2, y_2, z_2)$. Then, the spherical equation is

$$(x_1 - x_A)^2 + (y_1 - y_A)^2 + (z_1 - z_A)^2 = \frac{l^2}{4}, (x_2 - x_B)^2 + (y_2 - y_B)^2 + (z_2 - z_B)^2 = \frac{l^2}{4}. \quad (33)$$

The direction of fiber 1 is

$$\overrightarrow{AA_1} = (x_A - x_1, y_A - y_1, z_A - z_1). \quad (34)$$

The direction of fiber 2 is

$$\overrightarrow{BB_2} = (x_B - x_2, y_B - y_2, z_B - z_2). \quad (35)$$

Therefore, the inclined angle between the two fibers is

$$\theta = \arccos \frac{(x_A - x_1)(x_B - x_2) + (y_A - y_1)(y_B - y_2) + (z_A - z_1)(z_B - z_2)}{l^2/4}. \quad (36)$$

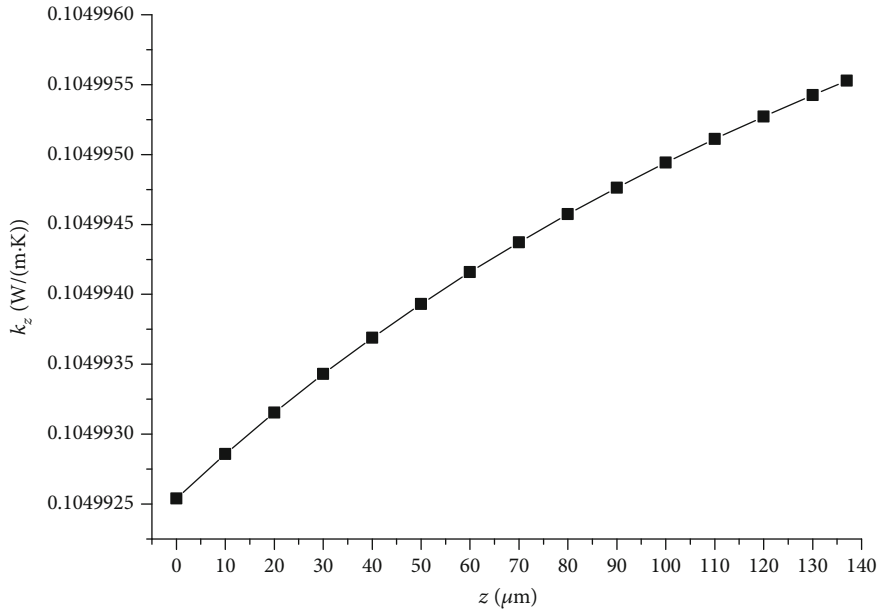

Figure 13: The influence of microsphere distance on heat transfer characteristics.

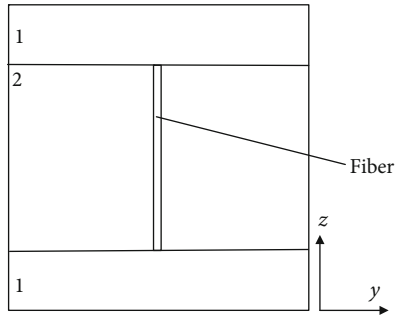

Figure 14: Unit cell model considering the fiber size.

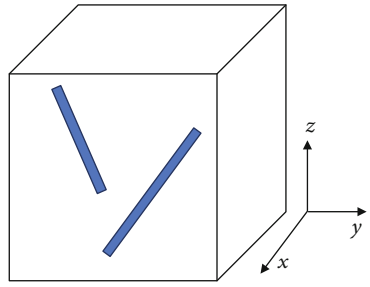

Figure 15: Unit cell model of fiber position relationship.

When the two fiber ends meet, then the intersection of spherical surface 1 and spherical surface 2 forms a circle of space. The equation is derived as follows:

$$\begin{cases} (x-x_A)^2+(y-y_A)^2+(z-z_A)^2=\dfrac{l^2}{4}, \\ (x-x_B)^2+(y-y_B)^2+(z-z_B)^2=\dfrac{l^2}{4}. \end{cases} \tag{37}$$

Then,

$$\begin{aligned} &2(x_B-x_A)x+2(y_B-y_A)y+2(z_B-z_A)z \\ &+x_A^2-x_B^2+y_A^2-y_B^2+z_A^2-z_B^2=0. \end{aligned} \tag{38}$$

This equation is the circular ring equation which is obtained by the two spherical surfaces intersecting. When two fibers are connected to the circular ring, the inclined angle is

$$\theta=\operatorname{arc}\frac{(x_A-x)(x_B-x)+(y_A-y)(y_B-y)+(z_A-z)(z_B-z)}{l^2/4}. \tag{39}$$

The parameters of x, y, and z in equation (39) satisfy equation (38). When two fibers translate to the intersect state, its inclined angle is the space angle of two fibers.

In order to intuitively describe influence of fiber distance and angle on thermal conductivity, two aspects were considered. First is the two fiber spatial disjunct, as shown in Figure 16(a), and the second is the two fiber intersect, including the endpoint connect, as shown in Figure 16(b). Figure 16(c) is the case that the rest part of the fiber is connected.

(2) The Relationship between Thermal Conductivity and Distance in Three Directions of Fiber. For two straight lines in space, they can determine a plane when they are shifted to the intersection state. So, two straight lines can only determine a plane which is parallel to the two straight lines. We can assume the two fibers parallel to the xy plane to establish a space rectangular coordinate system, as shown in Figure 17.

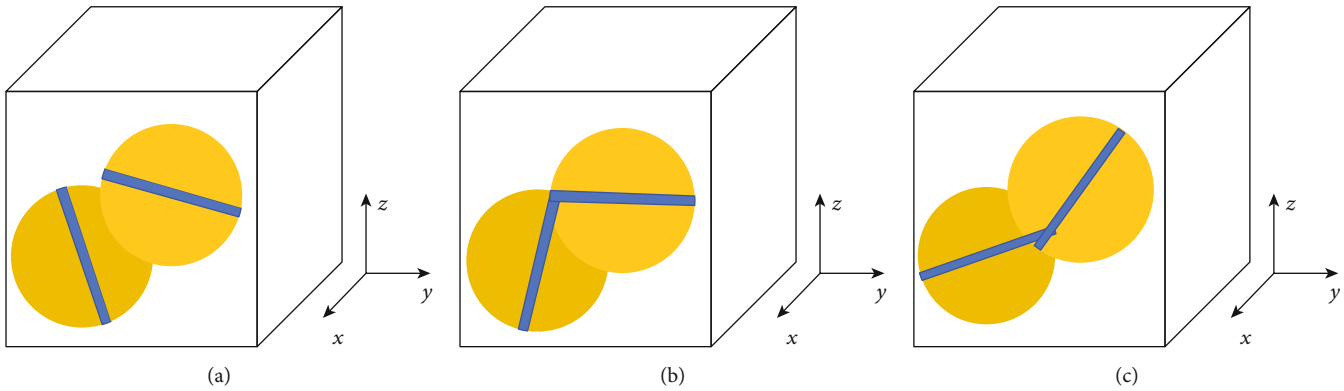

Figure 16: Spatial position relationship between two fibers.

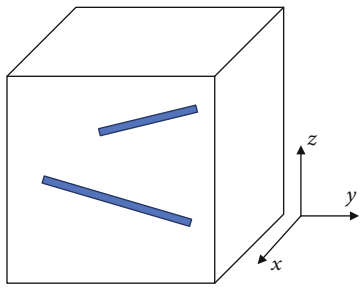

Figure 17: The distance relation model between fibers.

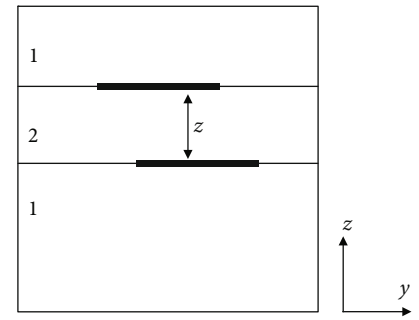

Figure 18: Front view diagram of the relationship between fibers.

(1) The Distance between the Fibers Varies in the z Direction. First, the influence of the change of distance in the z direction on the thermal conductivity along the z direction was studied when x and y remained unchanged. The distance in the x and y directions was taken to be the average distance, that is, $s_x = s_y = \bar{s}$. Figure 18 is the front view of the spatial distribution model of two fibers.

The distance between the fibers in the z direction is denoted as z. We assume that the fiber length is the same, denoting as l. The fiber is represented as cylinder, and the bottom radius is denoted as r; then, the equivalent thermal conductivity along the z direction is

$$k_z = \{(a - (z + 4r)/ak_m) + (a(z + 4r)^2/k_m\,(h_2a^2 - 2\pi r^2 l) + 2k_f\pi r^2 l)\}^{-1},$$

$$z \in [0, a - 4r]. \tag{40}$$

(2) The Distance between the Fibers Varies in the x Direction. The top view of the position relationship between the two fibers is shown in Figure 19.

In Figure 19, the inclined angle of two fibers is $\theta = \alpha + \beta$; α and β are the inclined angles of fiber 1 and fiber 2 in the y direction. The following is the discussion about the change of the thermal conductivity of the unit cell along the x direction with the distance x.

Here, the distance in the y direction is taken as the fixed value, that is, $y = \bar{s}$. It can be obtained from Figure 19 that the distance range of the two fibers in the x direction is

$$x \in \left[0, \frac{a - l(\sin\alpha + \sin\beta)}{2 - r(\sin\alpha + \sin\beta)}\right]. \tag{41}$$

So, the thermal conductivity of the unit cell along x direction is

$$k_x = \left\{\frac{a - [x + l(\sin\alpha + \sin\beta)/2 + r(\cos\alpha + \cos\beta)]}{k_m a} + \frac{a[x + l(\sin\alpha + \sin\beta)/2 + r(\cos\alpha + \cos\beta)]^2}{k_m[a^2(x + l(\sin\alpha + \sin\beta)/2 + r(\cos\alpha + \cos\beta)) - 2\pi r^2 l] + 2k_f\pi r^2 l}\right\}^{-1}, \tag{42}$$

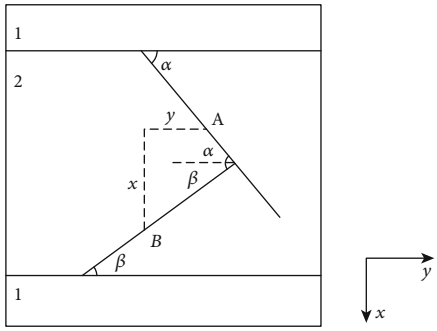

Figure 19: Top view of the relationship between fibers.

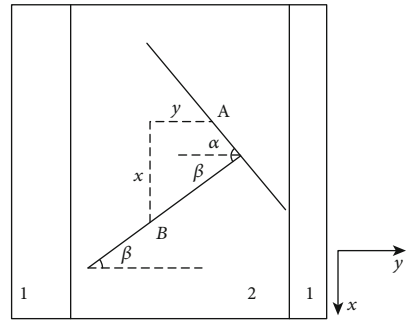

Figure 20: Top view of fiber distance in y direction.

(3) The Distance between the Fibers Varies in the y Direction. As shown in Figure 20, the distance between fibers in the x direction is kept constant, which is equal to the average distance between fibers. The change in the equivalent thermal conductivity of the unit cell in the y direction is discussed.

The value range of y is

$$y \in \left[0, \frac{a - l(\cos\alpha + \cos\beta)}{2 - r(\sin\alpha + \sin\beta)}\right]. \tag{43}$$

So, the equivalent thermal conductivity of the unit cell along y direction is

$$k_y = \left\{\frac{a - [y + l(\cos\alpha + \cos\beta)/2 + r(\sin\alpha + \sin\beta)]}{k_m a} + \frac{a[y + l(\cos\alpha + \cos\beta)/2 + r(\sin\alpha + \sin\beta)]^2}{k_m[a^2[y + l(\cos\alpha + \cos\beta)/2 + r(\sin\alpha + \sin\beta)] - 2\pi r^2 l] + 2k_f \pi r^2 l}\right\}^{-1}. \tag{44}$$

In order to study the relationship between the thermal conductivity of the unit cell in the y direction and the distance in the y direction, we assume $\alpha = \beta = \pi/8$ and substitute it into equation (44).

The curves of thermal conductivity changes in x, y, and z directions are shown in Figure 21 [25].

As can be seen from Figure 21, the equivalent thermal conductivity in x, y, and z directions increases with the distance, while the thermal conductivity in x and y directions is larger than that in z direction. When the distance increases to a certain extent, the thermal conductivity in the three directions tends to be the same.

(3) Effect of Fiber Space Angle on Thermal Conductivity. When the distance in the x, y, and z directions of the fibers remains the same, we take $x = y = z = \bar{s}$, the inclined angle changes. Since the xy plane of the coordinate system is parallel to the two fibers, the inclined angle of the two fibers is the inclined angle in the xy plane. When the inclined angle changes, the equivalent thermal conductivity in the z direction of the unit cell remains unchanged, while the thermal conductivity in the x and y directions changes with the inclined angle of the two fibers.

As the equivalent thermal conductivity along the x and y directions is also related to the angle between the two fibers and the y axis, without loss of generality, we can take this $\alpha = \beta = \theta/2$.

(1) Thermal Conductivity along x Direction. As shown in Figure 19, the equivalent thermal conductivity along x direction is

$$k_{ex} = \left\{\frac{a - [(a - 2d)/3 + l(\sin\alpha + \sin\beta)/2 + r(\cos\alpha + \cos\beta)]}{k_m a} + \frac{a[(a - 2d)/3 + l(\sin\alpha + \sin\beta)/2 + r(\cos\alpha + \cos\beta)]^2}{k_m[a^2[(a - 2d)/3 + l(\sin\alpha + \sin\beta)/2 + r(\cos\alpha + \cos\beta)] - 2\pi r^2 l] + 2k_f \pi r^2 l}\right\}^{-1}. \tag{45}$$

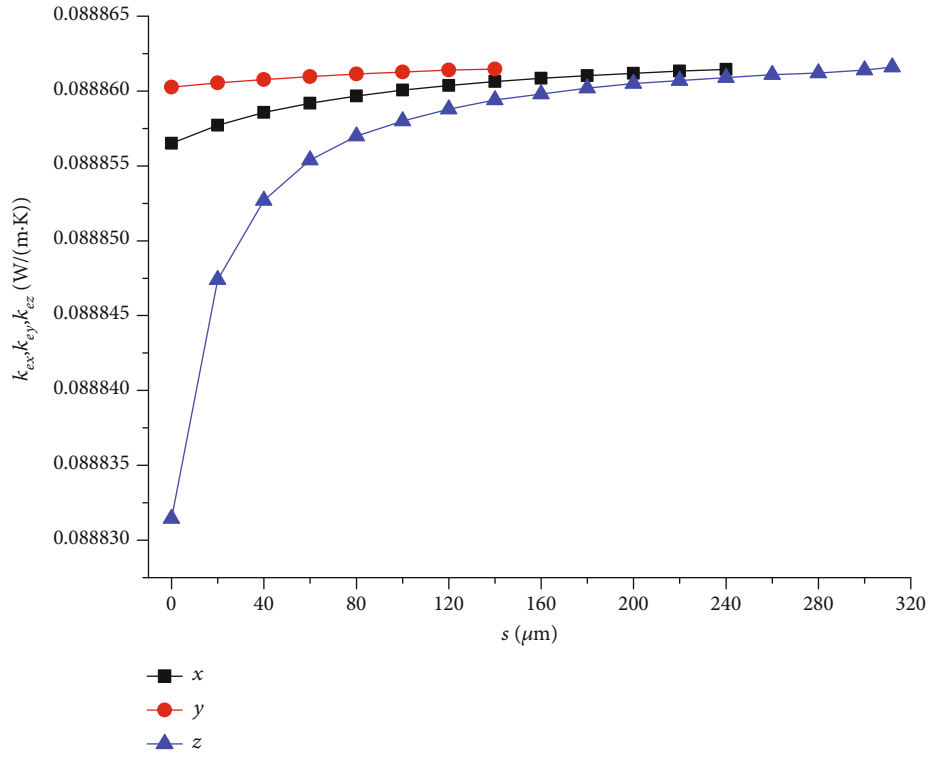

Figure 21: The relationship between thermal conductivity and distance in three directions of fiber.

Since the fiber orientation is stochastic, the fiber inclined angle obeys uniform distribution, and its probability density function is as follows:

$$f_x(\theta) = \frac{1}{\pi}, \quad \theta \in [0, \pi]. \tag{46}$$

Therefore, the equivalent thermal conductivity along x direction with probability and statistical significance is

$$\bar{k}_{ex} = \int_0^{\pi} k_{ex}(\theta) f_2(\theta) d\theta. \tag{47}$$

(2) Thermal Conductivity along y Direction. The derivation process of the thermal conductivity in the y direction is the same as that in the x direction, except that the trig function of the angle is different. The coefficient of thermal conductivity is as follows:

$$k_{ey} = \left\{ \frac{a - [(a-2d)/3 + l(\cos\alpha + \cos\beta)/2 + r(\sin\alpha + \sin\beta)]}{k_m a} + \frac{a[(a-2d)/3 + l(\cos\alpha + \cos\beta)/2 + r(\sin\alpha + \sin\beta)]^2}{k_m[a^2[(a-2d)/3 + l(\cos\alpha + \cos\beta)/2 + r(\sin\alpha + \sin\beta)] - 2\pi r^2 l] + 2k_f \pi r^2 l} \right\}^{-1}. \tag{48}$$

Since the fiber orientation is stochastic, the fiber inclined angle obeys uniform distribution, and its probability density function is as follows:

$$f_y(\theta) = \frac{1}{\pi}, \quad \theta \in [0, \pi]. \tag{49}$$

Therefore, the equivalent thermal conductivity along y direction with probability and statistical significance is

$$\bar{k}_{ey} = \int_0^{\pi} k_{ey}(\theta) f_3(\theta) d\theta. \tag{50}$$

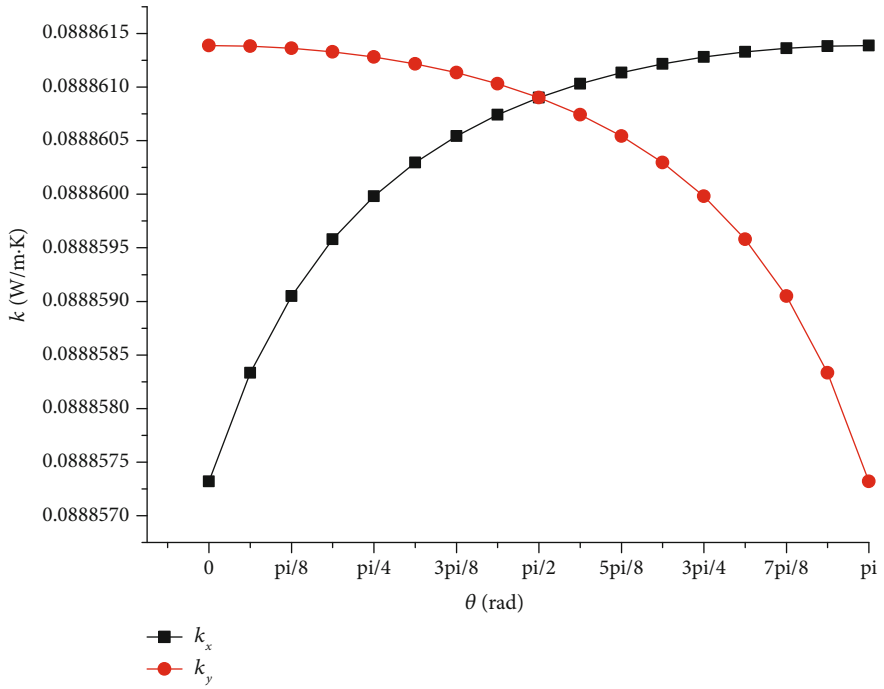

Figure 22: The relationship between the equivalent thermal conductivity in the x and y directions and the angle of fiber.

It can be seen from Figure 22 that the thermal conductivity is large when the heat transfer direction is consistent with the orientation of the fiber, while the thermal conductivity is small when the orientation of the fiber is perpendicular to the orientation of the heat transfer. This conclusion has been applied in thermal protection materials such as PICA. It is a new type of thermal protection material. The fiber distributes in the plane which is perpendicular to the direction of heat transfer. Fiber orientation with this plane is random, the space distance among fibers is very small, and although there is matrix filling, there are still a lot of pores. The distribution form of the fiber can greatly increase the complexity of the heat transfer path, so the heat transfer is blocked in the process of transmission; then, this microstructure can improve the thermal insulating capability significantly.

4.2.3. Effect of Fiber Thermal Conductivity and Volume Fraction. The effects of the fiber orientation angle, distance between fibers, and angle between fibers on the equivalent thermal conductivity of the unit cell were discussed from the perspective of fiber position relationship. As can be seen from the results, when the above parameters change, the equivalent thermal conductivity of the unit cell changes, but the amount of change is small. The first reason is that the thermal conductivity of the fiber is not particularly large compared with the matrix, and the second reason is that the volume content of the fiber is very small. The following two aspects are discussed to study the change of the equivalent thermal conductivity of the unit cell when the thermal conductivity of the fiber and the volume fraction change. Here, the orientation of a single fiber and the intersection of fibers are considered.

(1) The Orientation of a Single Fiber. Considering that the thermal conductivity of the fiber increases from 0.6 W/(m·K) to 80 W/(m·K), the equivalent thermal conductivity changes with the fiber orientation angle as shown in Figure 23.

As can be seen from Figure 23, when the thermal conductivity of the fiber is small, its orientation angle has little effect on the thermal conductivity of the unit cell. When it increases to more than 20 W/(m·K), its different orientation can significantly affect the equivalent thermal conductivity of the unit cell.

Next, the increase of fiber volume fraction will be discussed. As shown in Figure 24, when the thickness of the unit cell decreases along the x direction until it becomes the diameter of the fiber, the change of the equivalent thermal conductivity of the fiber along the z direction with the angle between the fiber and the z direction is shown in Figure 25. The thickness along the x direction is denoted as $xa, \boxtimes x \in [0.0352, 1]$. The equivalent thermal conductivity of the unit cell along the z direction is expressed as follows:

$$k_z = \left(\frac{a - (l\cos\theta + 2r\sin\theta)}{k_m a} + \frac{xa(l\cos\theta + 2r\sin\theta)^2}{k_m(xa^2(l\cos\theta + 2r\sin\theta) - \pi r^2 l) + k_f \pi r^2 l} \right)^{-1}. \quad (51)$$

It can be seen from Figure 25 that, when the unit cell is thin along the x direction, the fiber volume fraction is large, so the fiber orientation angle has a great influence on the

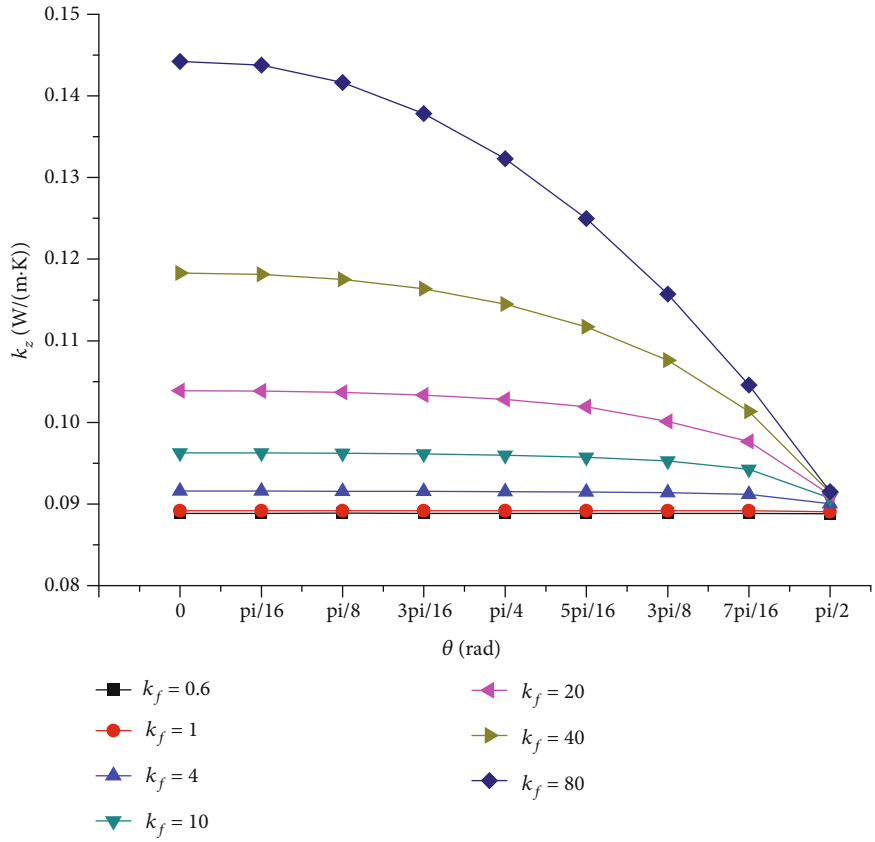

Figure 23: Effect of fiber thermal conductivity and orientation angle on equivalent thermal conductivity.

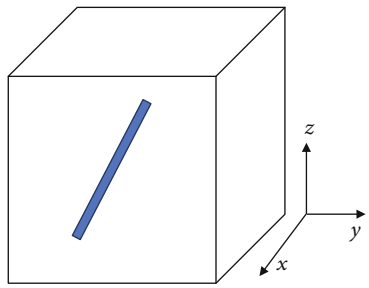

Figure 24: Fiber orientation model.

equivalent thermal conductivity of the unit cell. When x is 1, it is a cubic unit cell, and the volume fraction of the fiber is small, so the orientation of the fiber has very little effect on the equivalent thermal conductivity of the unit cell.

(2) Fiber Intersection. The fiber intersection model is shown in Figure 26, different thermal conductivities of fibers are considered here, and the equivalent thermal conductivity is shown as equation (52). The equivalent thermal conductivity along the z direction varies with the inclined angle, and the thermal conductivity of the fiber is shown in Figure 27:

$$k_{ez} = \left\{ \frac{a - l(\sin\alpha + \sin\beta)/2 - r(\cos\alpha + \cos\beta)}{k_m a} + \frac{a[l(\sin\alpha + \sin\beta)/2 + r(\cos\alpha + \cos\beta)]^2}{k_m[a^2(l(\sin\alpha + \sin\beta)/2 + r(\cos\alpha + \cos\beta)) - 2\pi r^2 l] + 2k_f \pi r^2 l} \right\}^{-1}. \quad (52)$$

As can be seen from Figure 27, when the thermal conductivity of the fibers is small, the fiber inclined angle has little effect on thermal conductivity of the unit cell. When it increases to more than 20 W/(m·K), the different inclined angles between the fibers can significantly affect the equivalent thermal conductivity.

When the thickness of the unit cell in the x direction which is shown in Figure 26 becomes smaller, that is, when

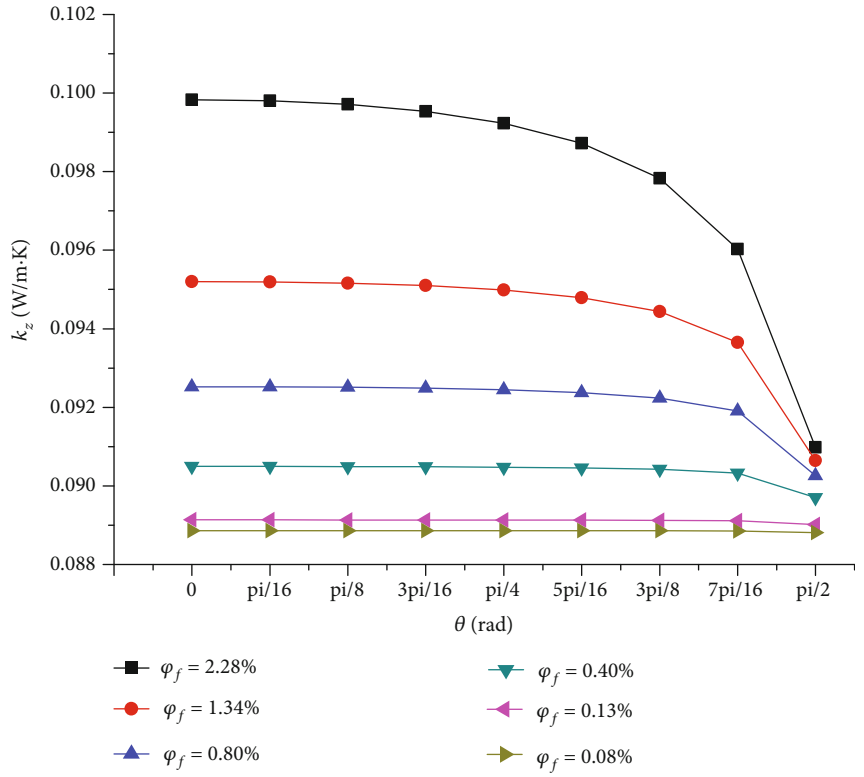

Figure 25: Effect of fiber volume fraction and orientation angle on thermal conductivity.

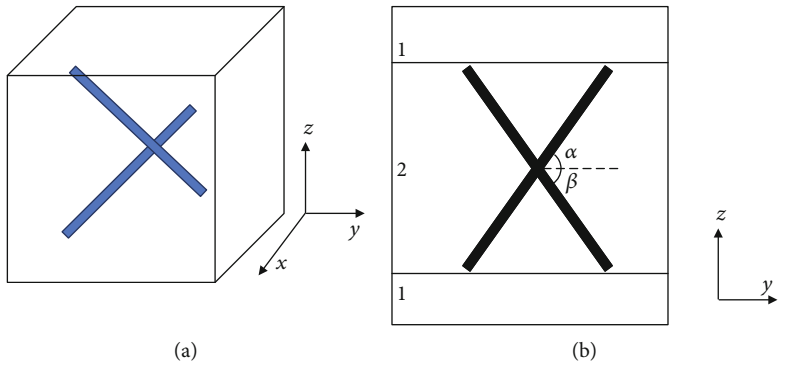

Figure 26: Fiber intersection model.

the volume fraction of the fiber increases, its equivalent thermal conductivity along the z direction can be expressed as

$$k_{ez} = \left\{ \frac{a - l(\sin\alpha + \sin\beta)/2 - r(\cos\alpha + \cos\beta)}{k_m a} + \frac{xa[l(\sin\alpha + \sin\beta)/2 + r(\cos\alpha + \cos\beta)]^2}{k_m[xa^2(l(\sin\alpha + \sin\beta)/2 + r(\cos\alpha + \cos\beta)) - 2\pi r^2 l] + 2k_f \pi r^2 l} \right\}^{-1}. \quad (53)$$

Different proportional coefficients were taken; that is, the fiber volume fraction in Figure 26 was 2.2849%, 1.3405%, 0.8043%, 0.4022%, 0.1341%, and 0.08043%, respectively. The unit cell gradually thickens along the x direction, so the fiber volume fraction decreases, and the change of the equivalent thermal conductivity of the unit

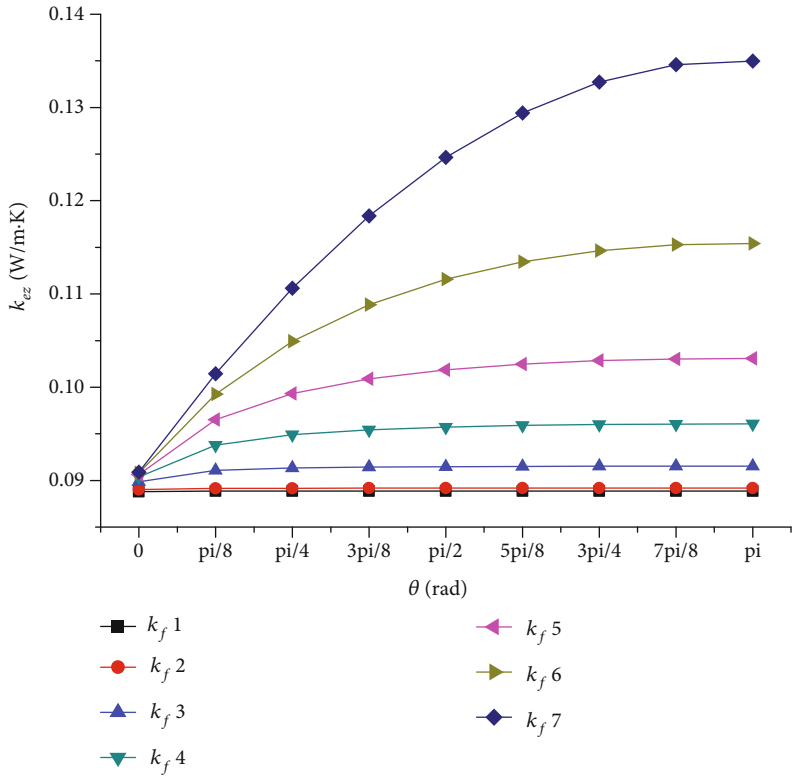

Figure 27: Effect of fiber thermal conductivity and fiber intersection angle on thermal conductivity.

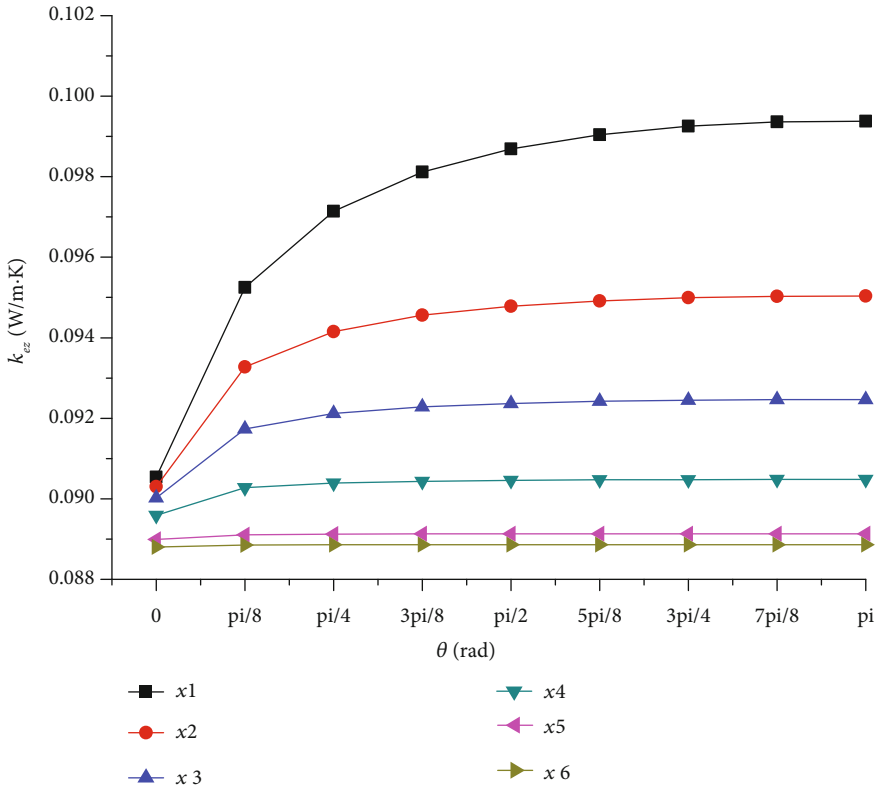

Figure 28: Effect of fiber volume fraction and fiber angle on thermal conductivity.

cell along the z direction with the inclined angle is shown in Figure 28.

When the x value is small, that is, when the unit cell is thin, the fiber volume fraction is large, so the angle between the fibers has a great influence on the equivalent thermal conductivity. When x is 1, it is a cubic unit cell, and the volume fraction of the fiber is small. Therefore, the angle between the fibers has very little effect on the equivalent thermal conductivity.

According to the analysis of the parameterization influence rule, the equivalent thermal conductivity is influenced greatly by the microstructure, and it is meaningful for the actual manufacturing process of ablative thermal insulating material. For example, we can use the hollow microspheres with low density and more and smaller microspheres to let them close to each other to make the equivalent thermal conductivity smaller. For fibers, they should be vertical to the heat transfer direction. In the actual manufacturing, when most fibers distribute randomly in the plane which is perpendicular to the heat transfer direction, the equivalent thermal conductivity will become smaller than other cases. So, the analysis of microstructural parameterization influence rule is meaningful for the manufacturing process improvement.

5. Conclusions

In this paper, the heat transfer characteristics of ablative thermal insulating materials at room temperature are analyzed, and the influence of various parameters on the thermal conductivity is discussed from two scales by establishing a kind of theoretical model. A fast method for predicting the heat transfer characteristics of ablative thermal insulating material was established. The conclusions are as follows:

(1) The mathematical model established in this article which is based on the law of minimal thermal resistance and the equal law of the specific equivalent thermal conductivity can get relatively accurate thermal conductivity prediction results. And the mathematical model can also obtain intuitive results of the parameterization influence rule of mesostructure

(2) At the microsphere scale, the equivalent thermal conductivity will decrease with the density, size, distribution area, and distance between microspheres decreasing

(3) At the fiber scale, the longer the heat transfer path along the direction of the fiber, the greater the equivalent thermal conductivity. As the thermal conductivity of fibers is larger than the matrix and microsphere, the equivalent thermal conductivity will increase with the increasing of fiber volume fraction and fiber thermal conductivity

(4) In the actual process of material technology design, the composite material with better performance can be designed considering the influence law of material microstructure parameters. Smaller equivalent thermal conductivity will be obtained if lower density and smaller size, distance, and distribution area of microspheres and fibers which distribute vertical to the heat transfer direction were adopted

Data Availability

(1) The data (table, figure, and curve graph) used to support the findings of this study are included within the article. (2) Previously reported data (table, curve graph, and SEM image) were used to support this study and are available at 10.1155/2019/8142532. These prior studies (and datasets) are cited at relevant places within the text as references [6, 7].

Conflicts of Interest

As authors, we certify that we have NO affiliations with or involvement in any organization or entity with any financial interest (such as honoraria; educational grants; participation in speakers' bureaus; membership, employment, consultancies, stock ownership, or other equity interest; and expert testimony or patent-licensing arrangements), or non-financial interest (such as personal or professional relationships, affiliations, knowledge or beliefs) in the subject matter or materials discussed in this manuscript.

Acknowledgments

The authors acknowledge the fund of the State Key Basic Research and Development Plan: 2015CB655201.

References

[1] R. E. Skochdopole, "The thermal conductivity of foam plastics," *Engineering Progress*, vol. 57, p. 55, 1962.

[2] J. C. Maxwell-Garnett, "Colours in metal glasses and in metallic films," *Philosophical Transactions of the Royal Society of London*, vol. 203, pp. 385–420, 1904.

[3] J. C. Maxwell, *A Treatise on Electricity and Magnetism*, Clarendon Press, 1904.

[4] C. W. Nan, "Physics of inhomogeneous inorganic materials," *Progress in Materials Science*, vol. 37, no. 1, pp. 1–116, 1993.

[5] J. C. Maxwell, *A Treatise on Electricity and Management*, Dover, New York, third edition, 1954.

[6] H. Fricke, "The Maxwell-Wagner dispersion in a suspension of ellipsoids," *The Journal of Physical Chemistry*, vol. 57, no. 9, pp. 934–937, 1953.

[7] D. P. H. Hasselman and L. F. Johnson, "Effective thermal conductivity of composites with interfacial thermal barrier resistance," *Journal of Composite Materials*, vol. 21, no. 6, pp. 508–515, 2016.

[8] D. Bruggeman, "Calculation of various physics constants in heterogenous substances I dielectricity constants and conductivity of mixed bodies from isotropic substances," *Annals of Physics*, vol. 24, no. 7, pp. 636–664, 1935.

[9] T. H. S. Sup, "Dielectric properties of emulsions," *Colloid & Polymer Science*, vol. 177, no. 1, pp. 57–61, 1961.

[10] K. Pietrak and T. S. Wiśniewski, "A review of models for effective thermal conductivity of composite materials[J]," *Journal of Power of Technologies*, vol. 95, no. 1, pp. 14–24, 2014.

[11] A. G. Every, Y. Tzou, D. P. H. Hasselman, and R. Raj, "The effect of particle size on the thermal conductivity of ZnS/diamond composites," *Acta Metallurgica et Materialia*, vol. 40, no. 1, pp. 123–129, 1992.

[12] S. Zhai, P. Zhang, Y. Xian, J. Zeng, and B. Shi, "Effective thermal conductivity of polymer composites: theoretical models and simulation models," *International Journal of Heat and Mass Transfer*, vol. 117, pp. 358–374, 2018.

[13] Z. Hashin and S. Shtrikman, "A variational approach to the theory of the effective magnetic permeability of multiphase materials," *Journal of Applied Physics*, vol. 33, no. 10, pp. 3125–3131, 1962.

[14] T. Mori and K. Tanaka, "Average stress in matrix and average elastic energy of materials with misfitting inclusions," *Acta Metallurgica*, vol. 21, no. 5, pp. 571–574, 1973.

[15] Y. Benveniste, "Effective thermal conductivity of composites with a thermal contact resistance between the constituents: nondilute case," *Journal of Applied Physics*, vol. 61, no. 8, pp. 2840–2843, 1987.

[16] Y. Agari, M. Tanaka, S. Nagai, and T. Uno, "Thermal conductivity of a polymer composite filled with mixtures of particles," *Journal of Applied Polymer Science*, vol. 34, no. 4, pp. 1429–1437, 1987.

[17] Y. Agari, A. Ueda, and S. Nagai, "Thermal conductivity of a polymer composite," *Journal of Applied Polymer Science*, vol. 49, no. 9, pp. 1625–1634, 1993.

[18] Y. Agari and T. Uno, "Estimation on thermal conductivities of filled polymers," *Journal of Applied Polymer Science*, vol. 32, no. 7, pp. 5705–5712, 1986.

[19] S. O. Zeng, A. Hunt, and R. Greif, "Geometric structure and thermal conductivity of porous medium silica aerogel," *Journal of Heat Transfer*, vol. 117, no. 4, pp. 1055–1058, 1995.

[20] Z. S. Cheng, J. Qian, and Y. H. Ye, "Theoretical calculation of equivalent thermal conductivity of composites," *Journal of University of Science and Technology of China*, vol. 22, no. 4, pp. 416–424, 1992.

[21] F. H. Li, *Study on heat transfer performance and mechanism of polymer / hollow microsphere composites*, South China University of Technology, Guangzhou, 2003.

[22] J. Z. Liang and G. S. Liu, "A new heat transfer model of inorganic particulate-filled polymer composites," *Journal of Materials Science*, vol. 44, no. 17, pp. 4715–4720, 2009.

[23] A. Alok and A. Satapathy, "Mathematical model for evaluating effective thermal conductivity of polymer composites with hybrid fillers," *International Journal of Thermal Sciences*, vol. 89, pp. 203–209, 2015.

[24] S. B. R. Devireddy and S. Biswas, "Physical and thermal properties of unidirectional banana–jute hybrid fiber-reinforced epoxy composites," *Journal of Reinforced Plastics and Composites*, vol. 35, no. 15, pp. 1157–1172, 2016.

[25] J. Gao, J. Yu, H. Han, and D. Deng, "Prediction of meso-heat transfer characteristics of resin-based ablative materials," *Acta Aeronautica et Astronautica Sinica*, vol. 38, no. z1, pp. 170-171, 2017.

[26] G. R. Cunnington, *Performance of multilayer insulation systems for temperatures to 700K, NASA CR-907*, NASA, Washing, D.C, 1967.